doi.org/10.36721/PJPS.2026.39.9.243.1

Network pharmacology combined with molecular docking to investigate the potential role of curcumin targeting TGR5 to modulate the GLP-1 pathway in T2DM with obesity

Chengyi Zhao and Juju Shang*
Cardiovascular, Beijing Hospital of Traditional Chinese Medicine, Beijing, 100010, China

Abstract: **Background**: In type 2 diabetes mellitus with obesity, both glycemic control and weight reduction are required; enhancing endogenous GLP-1 signaling has clinical value; TGR5 is an upstream target and the curcumin family has attracted attention but mechanistic evidence is scattered. **Objectives**: To evaluate, at structural and system levels, the mechanistic feasibility of the "curcumin–TGR5–GLP-1 axis" and to generate a prioritized ranking of candidates. **Methods**: Four human TGR5–Gs structures were used for redocking and Vina/GNINA consensus docking; based on the best poses, 200 ns×3 molecular dynamics (n=3) and MM-PBSA (100–200 ns) were performed; a GLP-1 module and a T2DM∩obesity network were constructed to conduct enrichment, proximity and randomization tests; receptor reachability was assessed by integrating ADMET and R_{direct} evidence was integrated according to preregistered weights. **Results**: Redocking validated reliability (9GYO pass rate 85.00%, RMSD = 0.86 A; 7CFN 75.00%, 1.17 Å; 7XTQ 65.00%, 1.39 Å). The consensus ranking was INT-777 > tetrahydrocurcumin > curcumin; demethoxycurcumin and bisdemethoxycurcumin tied, followed by curcumin-glucuronide and curcumin-sulfate. Molecular dynamics showed Hyd-W237/Hyd-F96 occupancy about 55%–79%, late-phase (100–200 ns) Hyd-L71 about 70%–81%; Hbond-Y240 about 28%–36%, Hbond-N93 in the late phase (100–200 ns) about 30%–36%, with key interactions stabilizing at 70–100 ns. MM-PBSA indicated INT-777 −28.94 kcal/mol, tetrahydrocurcumin −24.63, curcumin −18.72. Network statistics suggested closer inter-set adjacency: δ_obs = −0.53 (Z = −2.79, P_perm = 0.006), s_obs = −0.58 (Z = −2.76, P_perm = 0.008); enrichment was dominated by cAMP and Gαs-related pathways (q < 0.05). R_direct classified INT-777 = 0.78 and tetrahydrocurcumin = 0.64 as favorable, with all others < 0.50. **Conclusion**: Curcumin modulating the GLP-1 pathway via TGR5 is mechanistically feasible; tetrahydrocurcumin ranks superior across structural, system and reachability dimensions and is a prioritized candidate for experimental validation; conclusions are limited to binding feasibility, mechanistic indications and prioritization.

Keywords: Curcumin; GLP-1; Network pharmacology; TGR5

Submitted on 13-12-2025 – Revised on 05-01-2026 – Accepted on 15-01-2026

INTRODUCTION

Type 2 diabetes mellitus (T2DM) with obesity is characterized by insulin resistance, disordered energy metabolism and difficulty in weight control and management goals include not only achieving glycemic targets but also comprehensive improvement in body weight and cardiometabolic outcomes (Davies MJ *et al*., 2022). Drugs based on the GLP-1 pathway can achieve both glucose lowering and weight reduction. However, cost, tolerability and accessibility limit broad and long-term use, making induction of endogenous GLP-1 signaling a direction of practical significance (Rodriguez PJ *et al*., 2025). TGR5 is located in intestinal L cells; upon activation, it promotes GLP-1 secretion via the Gs-adenylyl cyclase-cAMP-PKA-CREB cascade and intertwines with bile acid metabolism and energy homeostasis (Fleishman and Kumar S, 2024). Curcumin and its metabolites have attracted attention in the metabolic field; previous reports suggest that they may influence the gut microbiota and bile acid profile, theoretically providing the possibility to link the TGR5 and GLP-1 axis (Tian F *et al*., 2023). Multiple human TGR5-Gs complex structures have been made publicly available, providing an operational basis to carry out rigorous structure-based computations at the level of the receptor's native conformation and to interface with system-level evidence (Yang F *et al*., 2020), Evidence around the curcumin-TGR5-GLP-1 axis remains fragmented, lacking parallel evaluation of direct action and system reachability under the same technical framework. Existing studies have not systematically answered whether curcumin and major metabolites can form stable occupancy in the TGR5 pocket, whether key interactions are consistent with known agonists, whether energetic and dynamic signals are concordant and whether, in the disease network, they are close to the GLP-1 module and genes related to T2DM with obesity (He Y *et al*., 2024; Jin W *et al*., 2024). Standardization of GLP-1-related gene sets and quantitative assessment of network proximity have also not been unified and the influence of permeability, efflux and metabolic constraints on the direct ligand path is often overlooked, resulting in a lack of reproducible basis for

**Corresponding author:* e-mail: sygqjuju@126.com.

candidate prioritization and the sequence of validation (Panossian A, 2025). At the translational level, there is an urgent need to center on three lines of evidence—receptor structure, system connectivity and receptor reachability—to form testable mechanistic hypotheses and a minimal verification checklist, thereby providing direction for subsequent design of functional experiments with practical feasibility and dosing optimization. This study aims to integrate molecular docking, molecular dynamics and MM-PBSA to validate, at structural and energetic levels, the binding feasibility on human TGR5 complexes; to conduct enrichment, proximity and randomization tests based on the protein-protein interaction network of the GLP-1 module and genes of T2DM with obesity; and, combined with ADMET and receptor reachability computations, to produce cross-structural and system-level evidence integration and candidate prioritization. Results present mechanistic indications under methodological consistency and propose a priority for tetrahydrocurcumin; conclusions are limited to testable mechanistic cues, serving subsequent minimal verification pathways and translational design.

MATERIALS AND METHODS

Study design

This study was a structural biology-driven, purely computational study and evidence synthesis. The objective was to evaluate, using a pre-specified workflow, the mechanistic feasibility and relative credibility of "curcumin targeting TGR5 to modulate the GLP-1 pathway in T2DM with obesity". The study protocol was locked before data freeze. The data freeze date was March 15, 2025 and the analysis period was March 16, 2025 to July 31, 2025. The operating system was Ubuntu 22.04.4 LTS. The main software and versions were: Python 3.11.9, R 4.3.3, RDKit 2023.09.3, Open Babel 3.1.1, AutoDock Vina 1.2.5, GNINA 1.0.3, GROMACS 2023.4, gmx_MMPBSA 1.5.9, Cytoscape 3.10.1, PROPKA 3.4.

Data sources and inclusion / exclusion criteria

Compound and metabolite data were obtained from structural entries in public chemical databases and standard names in the literature, with a freeze date of March 15, 2025. Disease and pathway gene sets were obtained from DisGeNET, GeneCards, Reactome, KEGG and Gene Ontology, with a freeze date of March 15, 2025. Protein structures were obtained from the Protein Data Bank. The protein-protein interaction network was obtained from STRING. *Inclusion criteria*: species restricted to Homo sapiens; structures or entries with clear identifiers and annotations; standardized IDs available and mappable to HGNC official gene symbols; PPI information had confidence scores and was filterable. *Exclusion criteria*: non-human entries; records missing core fields; duplicate records; records for which ID standardization could not be completed.

Sources of compound and metabolite data

The objects of study were restricted to curcumin, demethoxycurcumin, bisdemethoxycurcumin, tetrahydrocurcumin, curcumin-glucuronide and curcumin-sulfate. After obtaining SMILES, three-dimensional conformations were generated with RDKit using the ETKDG algorithm, with a maximum of 200 conformers and an energy window of 10 kcal/mol. Open Babel was used to generate major tautomers and ionization states at pH 7.4, retaining the most stable microstate. All small molecules were energy-minimized with MMFF94s to a gradient threshold of 0.1 $kcal \cdot mol^{-1} \cdot A^{-1}$.

Disease/pathway gene sets and PPI database

Genes related to T2DM and obesity were extracted from DisGeNET and GeneCards, respectively; high-confidence thresholds were set as DisGeNET gene-disease score ≥ 0.2 and GeneCards relevance score ≥ 10; after deduplication, the intersection was taken to form the "T2DM∩obesity" gene set (Piñero J *et al*., 2020). The PPI network was constructed based on STRING, using only Homo sapiens entries, with a combined score threshold set at ≥ 0.7 (STRING Consortium, 2026). The background gene set was defined as all human genes included in the PPI network.

Sources of TGR5 structures and reference ligands

Receptor structures were sourced from cryo-electron microscopy structures of human GPBAR1 (TGR5) active-conformation Gs complexes in the Protein Data Bank. Core structures used for the redocking benchmark and the main docking analyses were restricted to complex structures with resolution ≤ 3.6 A and containing co-crystallized ligands (at least two nonredundant ligand complexes); to supplement conformational coverage of the active conformation, 7BW0 (3.9 A; no co-crystallized-ligand coordinates available for redocking) was included as an auxiliary conformational reference and in sensitivity analyses we evaluated the impact on the main results and rankings of excluding this structure. Reference ligands included the known TGR5 agonist INT-777 and taurodeoxycholic acid derivatives. All PDB files were downloaded on the data freeze date and archived with original identifiers.

GLP-1 module definition and pathway baseline

The GLP-1 module was defined in a two-layer manner as "GLP-1 secretion and GLP-1 receptor signaling." The secretion-layer gene set included GCG, PCSK1, SLC2A2, KCNQ1, ABCC8, KCNJ11. The receptor-and-signaling-layer gene set included GLP1R, ADCY1, ADCY2, ADCY3, ADCY5, ADCY6, GNAS, PRKACA, PRKACB, PRKACG, PRKAR1A, PRKAR1B, PRKAR2A, PRKAR2B, RAPGEF3, RAPGEF4, CREB1, PDE3B, PDE4B. The inclusion rationale for these genes was their consistent recognition in mainstream pathway resources (Reactome/KEGG/GO) and canonical physiological

mechanisms as core nodes of GLP-1 biosynthesis/processing/secretion or of the GLP1R-Gs-cAMP-PKA/EPAC-CREB signaling cascade. To assess uncertainty introduced by manual curation, we tested alternative module definitions (e.g., retaining only the receptor-and-signaling layer or implementing minor expansions based on pathway annotations); after recalculation, key enrichment and network proximity results remained qualitatively consistent, indicating that the main findings were robust to module composition. All genes were converted to official HGNC symbols, manually verified and then fixed. This module served throughout the study as a predefined reference for enrichment analyses and network proximity statistics.

Structural modeling and molecular docking

Selection of receptor structures and pocket definition

Human TGR5–ligand–Gs complexes in the PDB were used and processed in the following order: non-structural heteroatoms were removed while co-crystallized ligands were retained; missing side chains and short missing loops were repaired with MODELLER; PROPKA predicted pKa and assigned protonation states at pH 7.4; His residues were assigned HID or HIE based on hydrogen-bond geometry and the protonation microenvironment; disulfide bonds were retained. The docking grid center was set at the center of mass of the co-crystallized ligand, with a grid box side length of 24 A and each axis extended outward by 6 A to cover the pocket.

Redocking benchmark and positive control

Redocking with the co-crystallized ligand was used to evaluate the effectiveness of the grid and parameters. The heavy-atom RMSD threshold between redocked poses and crystal poses was set to ≤ 2.0 A (Zheng L *et al*., 2022). The positive-control molecules INT-777 and tauro-bile acid agonists were subjected to the same workflow to verify scoring and interaction patterns.

Formal docking and consensus scoring

AutoDock Vina and GNINA were used for parallel docking. Vina parameters: exhaustiveness = 32, num_modes = 20, energy_range = 4 kcal/mol. GNINA used the default CNN scoring and output the Top 20 poses (Eberhardt J *et al*., 2021). All conformers of all compounds were docked and deduplicated; a consensus score across engines was computed using a weighted rank-sum method, with weights set to Vina: GNINA = 1:1. Poses entering subsequent analyses were required to meet both criteria: top 10% by consensus and cross-engine pose RMSD ≤ 2.0 Å. Hydrogen bonds, salt bridges, hydrophobic clamping and π-stacking interactions with key pocket residues were recorded; a distance threshold of 2.5-3.5 A was used to determine hydrogen-bond donors/acceptors and ≤ 4.5 A was used as the threshold for hydrophobic contacts (Leidner F *et al*., 2019).

Molecular dynamics simulations

System construction and running parameters

For each compound, the consensus best pose was selected to construct the TGR5–ligand complex system. The membrane environment was a POPC bilayer. The force field was CHARMM36m (protein and lipids), the water model was TIP3P and small-molecule parameters were generated by CGenFF; if any force-field penalty score was > 50, B3LYP/6-31G geometry optimization was performed and charges were fit by RESP before regenerating parameters. After solvation, the system was neutralized with 0.15 mol/L NaCl. Energy minimization used 5,000 steps of steepest descent; the equilibration stage was performed under NVT for 1 ns and NPT for 5 ns, with positional restraints gradually released. In the production stage, each system ran 3 independent replicate trajectories, every 200 ns, with an integration time step of 2 fs, temperature 310 K (velocity-rescale thermostat), pressure 1 bar (Parrinello–Rahman barostat), long-range electrostatics treated with PME, Coulomb and van der Waals cutoffs of 1.2 nm and hydrogen bonds constrained by LINCS.

Trajectory analysis and stability assessment

Analysis metrics included: hydrogen-bond occupancy between ligand and pocket residues, frequency of hydrophobic contacts, ligand heavy-atom RMSD, pocket-residue RMSF and pocket volume fluctuations. Binding free energy was estimated with gmx_MMPBSA by performing MM-PBSA on 50 conformations sampled at equal intervals within the last 100 ns of the production phase, reporting relative binding energy and standard error, with the statement that this estimate was used for relative ranking.

Network pharmacology and system analysis

Construction of the curcumin target set

Known targets of curcumin and the above metabolites were extracted from ChEMBL and the Comparative Toxicogenomics Database. Inclusion criteria were human targets with functional or binding evidence; pChEMBL ≥ 5 in ChEMBL; evidence type of direct action in CTD. All targets were unified to HGNC official symbols.

PPI network and pathway enrichment

A PPI network was constructed in STRING with a combined score ≥ 0.7 and, within this network background, Reactome, KEGG, and GO enrichment were performed for the “curcumin target set”, the “GLP-1 module” and the “T2DM∩obesity gene set” separately and their union. The R package clusterProfiler was used; enrichment tests employed the hypergeometric distribution, with the Benjamini–Hochberg method controlling FDR. The significance threshold was set at FDR < 0.05.

Network proximity and randomization tests

Network proximity and separation s between sets were calculated based on shortest paths and 10,000 degree-

preserving random permutations were performed to generate the null distribution, reporting z scores and two-tailed P values. The significance threshold was set at $P < 0.05$ and $|z| \geq 1.96$.

ADMET and receptor reachability assessment

SwissADME, pkCSM and ADMETlab 3.0 were used under pH 7.4 conditions to predict oral absorption, Caco-2 permeability, P-gp substrate status, plasma protein binding, CYP3A4- and UGT-related metabolic risk, aqueous solubility and LogP. Combined with the basolateral membrane localization of TGR5 in intestinal L cells, a "direct reachability decision table" was constructed; the three dimensions of membrane permeability, efflux risk and metabolic stability were each normalized to 0-1 with 0.5 used as the threshold to determine favorable or unfavorable *(Brighton CA et al., 2015).*Accordingly, a composite direct reachability score R_direct (0.4 × normalized permeability + 0.3 × [1 − normalized efflux risk] + 0.3 × normalized metabolic stability) was calculated and used to prioritize the relative reachability of candidate molecules in the "direct ligand path." Considering that curcumin-class compounds have been reported to have pharmacokinetic constraints such as limited oral exposure, conjugative metabolism (e.g., UGT/SULT) and efflux, this study used R_direct as a relative indicator of reachability constraints rather than as a quantitative predictor of *in-vivo* exposure. The binding energy estimation of MM-PBSA adopted a single-trajectory scheme (extracting receptor and ligand conformations from the same complex trajectory for calculation) and the entropy term (-TΔS) was not explicitly included; this setting was used for relative ranking of candidate molecules within the same receptor pocket to reduce the computational cost and uncertainty introduced by entropy estimation.

Evidence integration, statistics and sensitivity analyses

Four lines of evidence were standardized to z-scores: consensus docking ranking, MD stability metrics (a joint z-score of hydrogen-bond occupancy and MM-PBSA relative binding energy), network-level evidence (a joint z-score of enrichment and proximity of the GLP-1 module and T2DM∩obesity) and the ADMET reachability composite score. A weighted sum was used to form the "direct ligand path total score," with weights set as structural docking 0.30, MD stability 0.25, network-level 0.25 and ADMET 0.20. These weights were a predefined prior setting (locked before the data freeze), mainly reflecting the relative importance and uncertainty of different evidence in the research chain for the "direct ligand path": structural docking and MD/MM-PBSA correspond more directly to "ligand-TGR5 binding and stability," hence slightly higher weights; network evidence is used to verify system connectivity in the context of the GLP-1 module and T2DM∩obesity and belongs to mechanistic support evidence, with a mid-level weight; ADMET/R_direct is used to assess receptor reachability but is based on predictive models with relatively higher extrapolation uncertainty, thus a slightly lower weight. Robustness was examined with two sensitivity schemes: multi-scenario analysis with ±20% weight perturbations and leave-one-out cross-validation. For the "indirect modulation path," a separate system-level evidence score centered on enrichment of bile acid metabolism and FXR/TGR5-related pathways was calculated and presented alongside the direct path total score. All statistical tests were two-tailed; the significance threshold (where applicable) was set at $P < 0.05$ and the FDR control threshold was set at < 0.05. Effect sizes (enrichment strength, proximity difference, MM-PBSA relative energy difference) and 95% confidence intervals were reported simultaneously.

RESULTS

Pathway evidence baseline

After systematic retrieval and strict screening, 25 genes were finally included in the GLP-1 module (6 in the secretion layer and 19 in the receptor-and-signaling layer), providing a clear and robust genetic basis for subsequent molecular docking and network pharmacology analyses (Fig. 1). Among them, the receptor-and-signaling layer contained the ADCY family (ADCY1/2/3/5/6, 5 in total), PKA subunits (PRKACA/PRKACB/PRKACG and PRKAR1A/1B/2A/2B, 7 in total), PDE cAMP hydrolases (PDE3B, PDE4B, 2 in total), EPAC (RAPGEF3, RAPGEF4, 2 in total) and core signaling nodes (GLP1R, GNAS, CREB1, 3 in total); the secretion layer included GCG, PCSK1, ABCC8, KCNJ11, KCNQ1 and SLC2A2. The complete gene list and sources of evidence are provided in the Table S1.

Receptor structure preparation and benchmark validation

This study used four human TGR5–Gs cryo-electron microscopy complex structures: PDB 9GYO (2.5 Å; EMDB EMD-51700), 7CFN (3.0 Å; EMDB EMD-30345), 7XTQ (3.2 Å; EMDB EMD-33452) and 7BW0 (3.9 Å; EMDB EMD-30221). The molecular docking grid was centered at the center of mass of the co-crystallized ligand, with a box side length of 20.5–24.0 A and optimized in 0.5 Å steps (Table 1). After calculating 95% confidence intervals using the Clopper–Pearson method, redocking results for the three TGR5 structures showed that 9GYO had the highest pass rate (85.00%, RMSD = 0.86 A), followed by 7CFN (75.00%, RMSD = 1.17 Å) and 7XTQ was slightly lower (65.00%, RMSD = 1.39 Å). All met the RMSD ≤ 2.0 Å criterion, validating the reliability of the receptor conformations and grid parameters (Fig. 2). Complete experimental methods are provided in Table S2.

Molecular docking results

The consensus ranking (Vina+GNINA rank-sum normalization) was, in order: INT-777, tetrahydrocurcumin, curcumin, demethoxycurcumin and bisdemethoxycurcumin (tied for 4th), with curcumin-glucuronide and curcumin-sulfate ranking lower (Fig. 3).

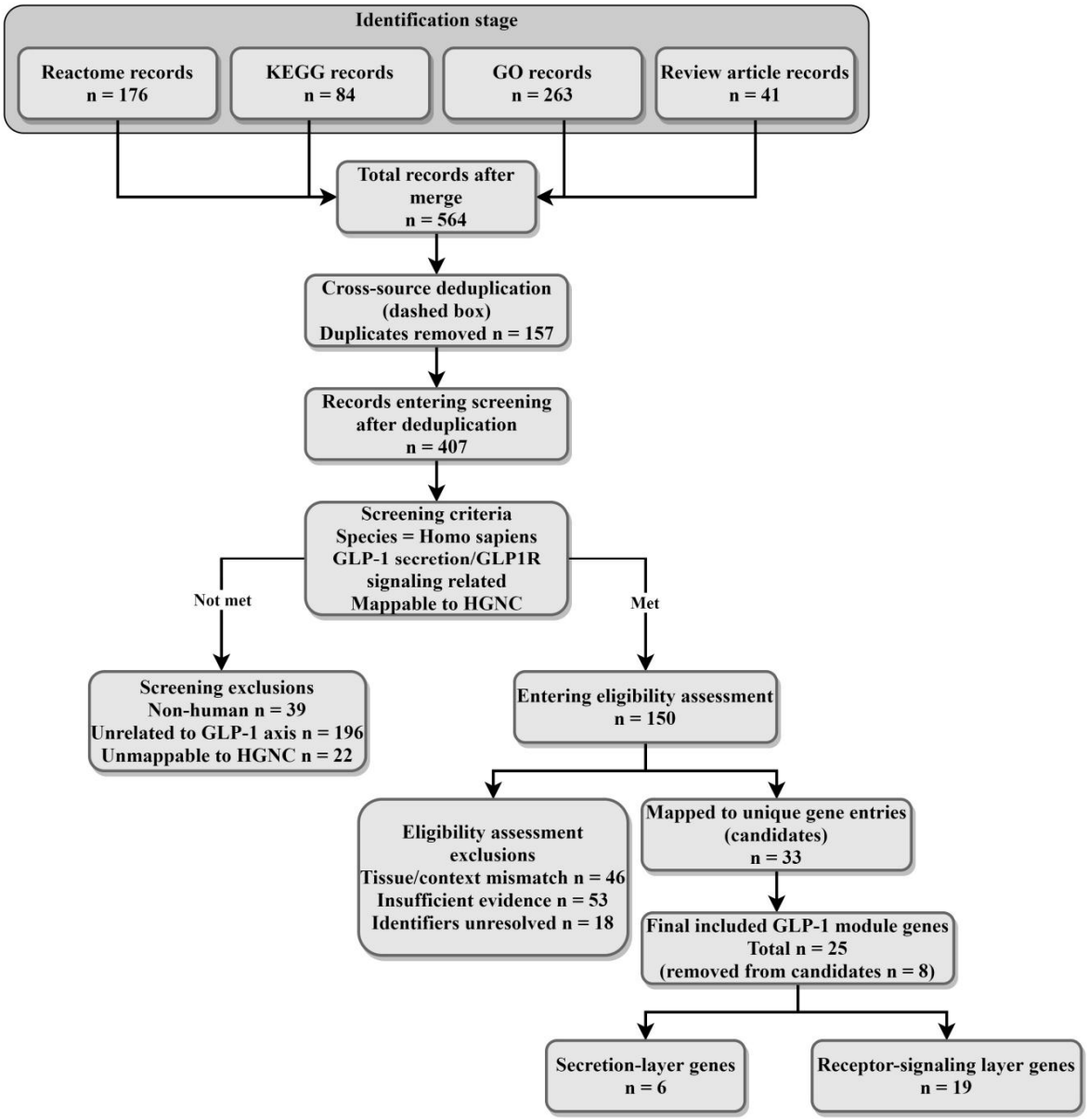

Fig. 1: Gene-set curation and inclusion workflow.

Table 1: List of included human TGR5–ligand complex structures and quality metrics

PDB ID	EMDB ID	Map resolution A	Co-crystallized ligand	Chain length	Missing residues	Repaired segments	Histidine protonation	Docking grid center x, y, z (A)	Grid box size (A×A×A)
9GYO	EMD-51700	2.5	FWX	330	E:1–2 (2); E:327–330 (4)	None	45659	11.8, −15.7, 22.5	20.5×20.5×20.5
7CFN	EMD-30345	3.0	FX0 (INT-777)	330	E:1–4 (4); E:233–237 (5); E:323–330 (8)	E:233–237 (5)	45659	13.4, −11.2, 25.7	22.0×22.0×22.0
7XTQ	EMD-33452	3.2	H8I (R399)	330	E:1–5 (5); E:236–240 (5); E:324–330 (7)	E:236–240 (5)	45689	15.1, −8.3, 27.6	23.5×23.5×23.5
7BW0	EMD-30221	3.9	None (23H not modeled in coordinates)	302 (R:6–307)	R:1–5 (5); R:238–242 (5); R:308–330 (23)	R:239–241 (3)	45658	14.0, −10.5, 26.1	24.0×24.0×24.0

Note: Protonation states were determined by PROPKA at pH 7.4.

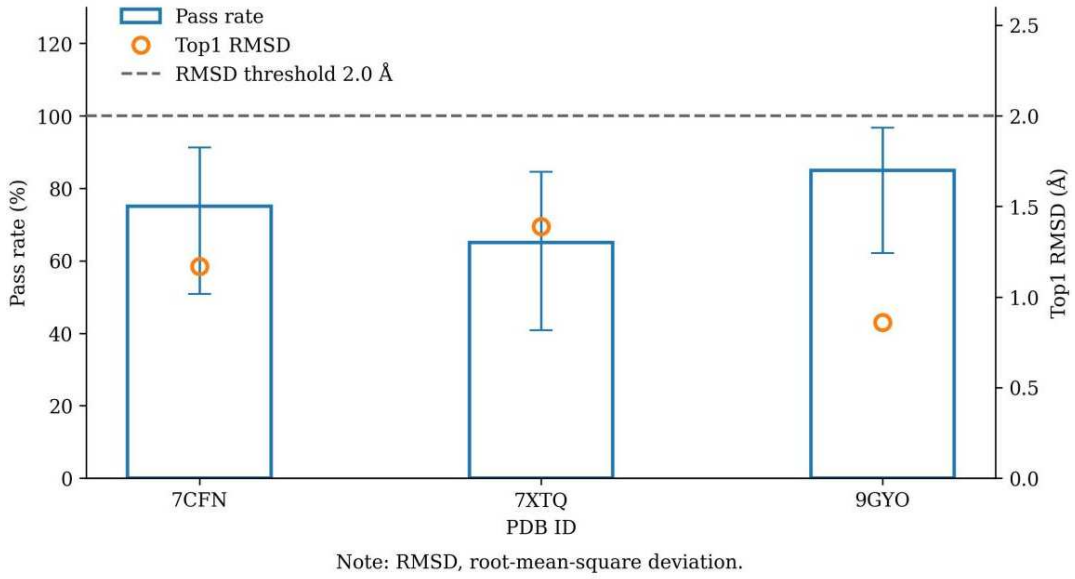

Fig. 2: Bar chart of ligand RMSD and pass rate for the redocking benchmark

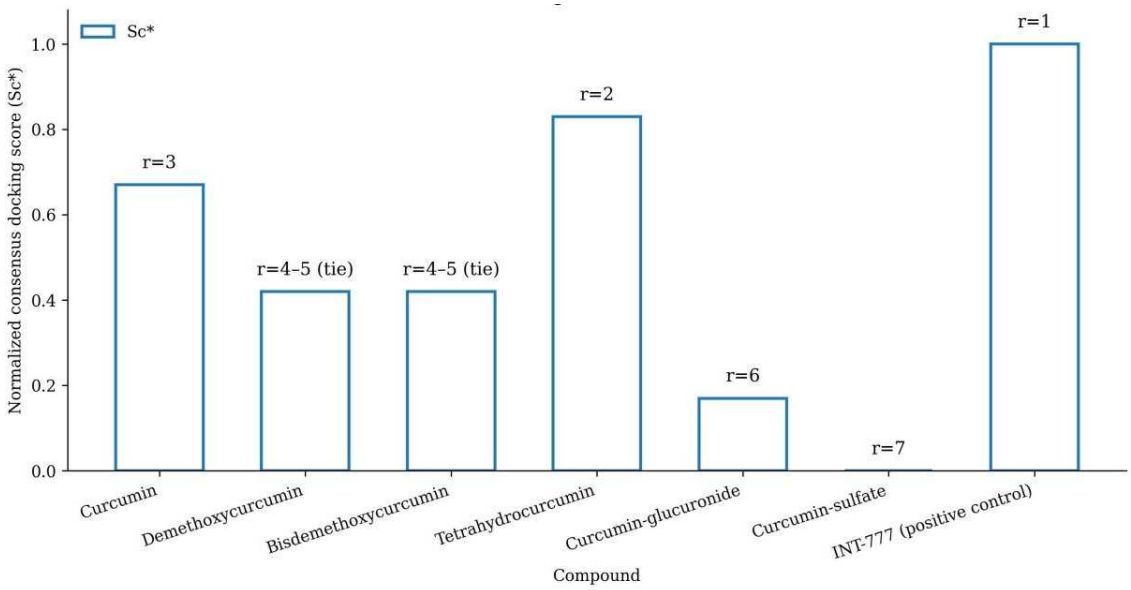

Fig. 3: Bar chart of consensus docking scores and relative rankings of curcumin and metabolites on TGR5

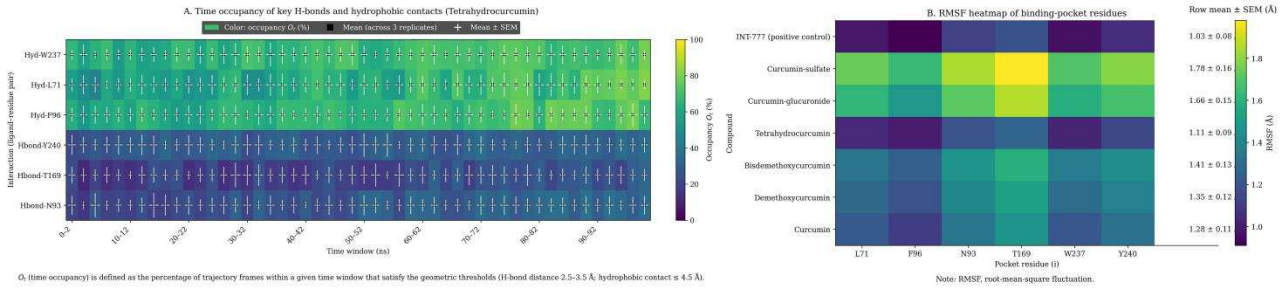

Fig. 4: Stability and flexibility of ligand–TGR5 pocket interactions. (A) Time occupancy of key H-bonds and hydrophobic contacts; (B) RMSF heatmap of binding-pocket residues.

Molecular dynamics stability and binding energy

Based on geometric thresholds during the MD production period (100 ns), hydrophobic contacts between tetrahydrocurcumin and the TGR5 pocket were dominated by Hyd-W237 and Hyd-F96 (approximately 55%–79%), with Hyd-L71 increasing markedly in the late phase (approximately 70%–81%); hydrogen bonds were dominated by Hbond-Y240 (approximately 28%–36%), followed by Hbond-N93 (approximately 30%–36% in the late phase), while Hbond-T169 was lower (approximately 15%–30%). Overall, key interaction events tended to stabilize at 70–100 ns (Fig. 4A). Based on Cα atom RMSF (100 ns, three replicates), overall pocket fluctuation from low to high was: INT-777 (1.03 ± 0.08 A) < tetrahydrocurcumin (1.11 ± 0.09 A) < curcumin (1.28 ± 0.11 A) < demethoxycurcumin (1.35 ± 0.12 A) < bisdemethoxycurcumin (1.41 ± 0.13 A) < curcumin-glucuronide (1.66 ± 0.15 A) < curcumin-sulfate (1.78 ± 0.16 A); at the site level, W237 and F96 showed the lowest fluctuation, T169 the highest and N93 and Y240 were intermediate (Fig. 4B). Using MM-PBSA (100–200 ns; 50 snapshots at equal intervals per trajectory; n = 3; BCa 95% CI), DeltaG_bind from low to high were: INT-777 (−28.94), tetrahydrocurcumin (−24.63), curcumin (−18.72), demethoxycurcumin (−16.38), bisdemethoxycurcumin (−15.94), curcumin-glucuronide (−9.21), curcumin-sulfate (−7.83) (Table 2).

Network pharmacology and system-level evidence

In the maximum connected subnetwork constructed with STRING ≥ 0.70, GNAS was the highest-degree node (5), followed by PRKACA and CREB1 (4); TGR5 was directly connected to GNAS and GLP1R–GNAS–ADCY3/5/6 formed the Gs–AC backbone; the intersection nodes PPARG and ADCY5 were highlighted and the network realized concentrated connections among curcumin targets, the GLP-1 module and the T2DM∩obesity genes (Fig. 5). By hypergeometric test with BH correction, the most significantly enriched pathway was the cAMP signaling pathway, followed by G alpha s signalling events and GPCR downstream signalling; Gs activates adenylyl cyclase, PI3K–Akt signaling pathway and GLP-1 regulates insulin secretion were also among the top (all $q < 0.05$), suggesting that curcumin may modulate T2DM with obesity through these pathways (Table 3). In 10,000 degree-preserving randomization tests (all $P_{perm} < 0.05$ and $|Z| \geq 1.96$), key nodes were mainly focused on the Gs–cAMP–PKA–CREB axis: GNAS had the highest shortest-path contribution (SPC = 38.26%), followed by PRKACA (33.41%) and CREB1 (31.07%); ADCY5, ADCY3, PDE3B, PRKAR2B, GLP1R, AKT1 and PPARGC1A also made significant contributions (SPC range 14.22–27.92%) (Table 4).

Network proximity and randomization tests

Based on 10,000 degree-preserving randomizations, the observed values were $\delta_{obs} = -0.53$ ($Z = -2.79$, $P_{perm} = 0.006$) and $s_{obs} = -0.58$ ($Z = -2.76$, $P_{perm} = 0.008$); both were < 0 and fell outside the 95% interval of the null distribution, indicating that inter-set distances were lower than random expectation (Fig. 6).

ADMET and receptor reachability

Using the R_direct composite score (0.4 × normalized permeability + 0.3 × [1 − normalized efflux risk] + 0.3 × normalized metabolic stability, threshold 0.50), the results showed INT-777 (0.78) and tetrahydrocurcumin (0.64) classified as favorable (both R_direct > 0.5); curcumin, demethoxycurcumin, bisdemethoxycurcumin, curcumin-glucuronide and curcumin-sulfate were all unfavorable (all R_direct < 0.5) (Table 5).

Evidence integration and path trade-offs

Combining structural evidence ($S_{struct} = 0.30 \times Z_{dock} + 0.25 \times Z_{MD}$) and system evidence ($S_{syst} = 0.25 \times Z_{net} + 0.20 \times Z_{ADMET}$), a two-dimensional scatter plot was drawn with a Hotelling T^2 95% confidence ellipse. The results showed that the positive control INT-777 was located in the upper right region; the metabolite tetrahydrocurcumin followed; parent curcumin was in the middle; demethoxycurcumin and bisdemethoxycurcumin were in the lower right; curcumin-glucuronide and curcumin-sulfate were in the lower left (Fig. 7).

Sensitivity and robustness analysis

Deterministic recalculation and Spearman rank correlation assessment indicated that the baseline scenario favored Direct; ±20% weight perturbations (14 scenarios in total) were all stable in Direct favored or tied, with no scenario shifting to Indirect; leave-one-out switched to Indirect favored only when the dock weight was removed. Spearman ρ of perturbation scenarios was 0.94–0.96 and for leave-one-out was 0.82–0.88; DeltaRank ranged from −2 to +2. Complete data are provided in the Table S3.

DISCUSSION

Redocking pass rate and ligand heavy-atom RMSD were within acceptable ranges, suggesting that receptor conformations and grid parameters were reliable; the consensus docking ranking placed the positive control agonist highest, tetrahydrocurcumin second and curcumin next; in molecular dynamics simulations, key hydrophobic interactions were dominated by W237 and F96, with L71 increasing its involvement in the later phase and Y240 forming a stable hydrogen bond, with key interactions tending to plateau in the second half of the simulations; pocket-residue RMSF from low to high corresponded to the positive agonist, tetrahydrocurcumin, curcumin and its metabolites and the MM-PBSA binding free energy ranking was consistent with the above results (Torrens-Fontanals M *et al*., 2020).

Table 2: MM-PBSA relative binding free energy

Compound	DeltaG_bind (kcal/mol)	95% CI (kcal/mol)
INT-777 (positive control)	-28.94	-31.22 to -26.41
Tetrahydrocurcumin	-24.63	-27.05 to -22.44
Curcumin	-18.72	-21.03 to -16.11
Demethoxycurcumin	-16.38	-18.97 to -14.12
Bisdemethoxycurcumin	-15.94	-18.20 to -13.41
Curcumin-glucuronide	-9.21	-11.58 to -7.02
Curcumin-sulfate	-7.83	-10.27 to -5.46

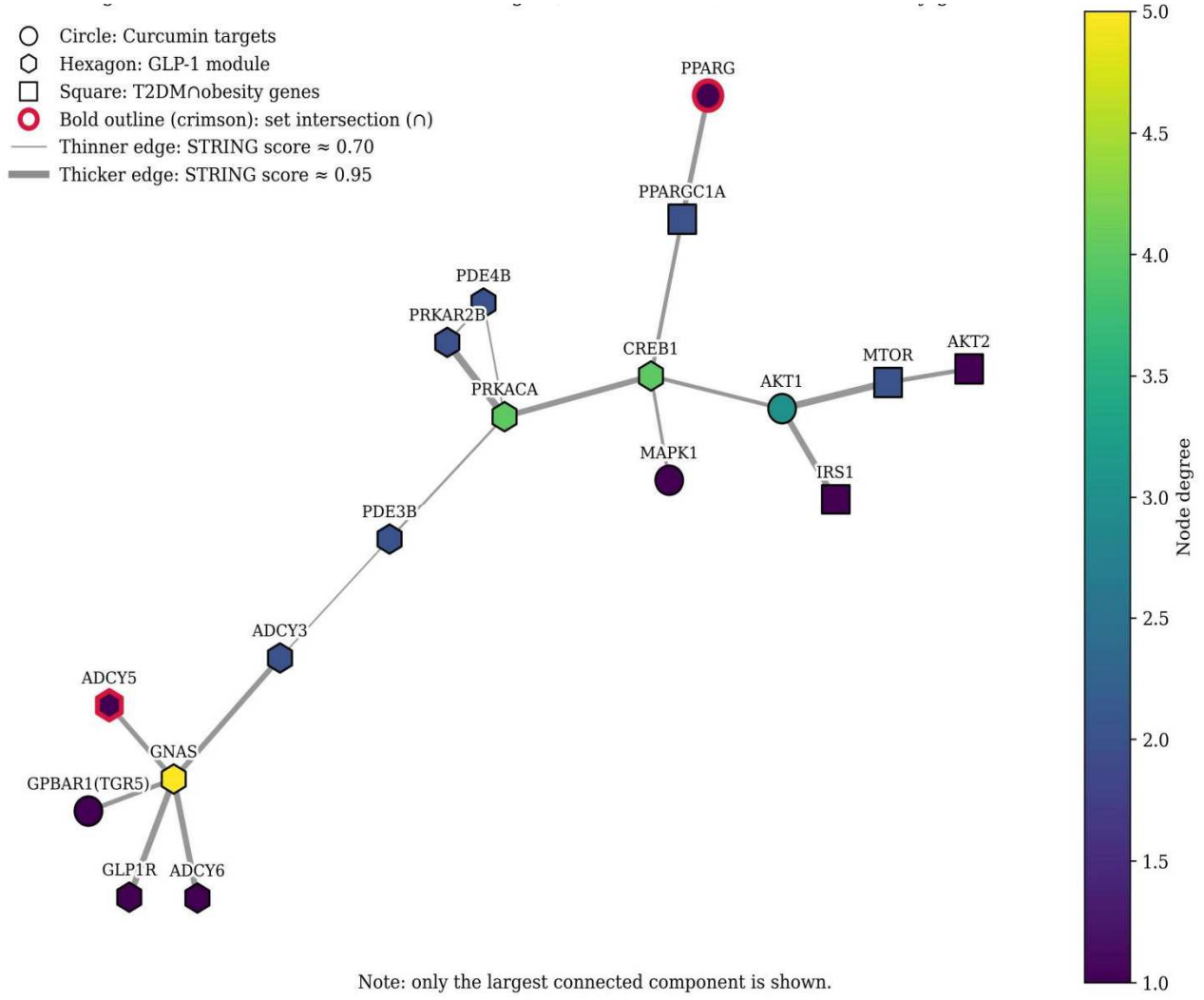

Fig. 5: Integrated PPI subnetwork of curcumin targets, GLP-1 module and T2DM∩obesity genes

These results together suggest that structural features of the activated TGR5 pocket provide clamping and desolvation effects for a deep hydrophobic cavity, with a few polar sites responsible for anchoring, among which W237, F96 and L71 provide stability and Y240 contributes directional constraints *(Ma L et al., 2022);* tetrahydrogenated molecules are closer to the bile acid-like scaffold in steric and hydrophobic matching and reduced planarity and a more freely distributed set of rotatable bonds facilitate conformational accommodation in the pocket, thereby achieving greater stability and energetic advantage than the parent compound *(González Y et al., 2023)*; the parent curcumin shows suboptimal local flexibility and geometric matching to the pocket and conjugated metabolites have lower stability due to charge and solvation *(Bertoncini-Silva C et al., 2024).*

Table 3: Reactome and KEGG pathway enrichment results

Pathway name	Database	Pathway ID	Gene count (k)	Generatio (k/|Query|)	Bgratio (K/|Background|)	OR	P value	FDR q
cAMP signaling pathway	KEGG	hsa04024	6	6/18	200/18873	14.82	0.001	0.006
G alpha s signalling events	Reactome	R-HSA-418555	5	5/18	96/18873	16.83	0.001	0.007
GPCR downstream signalling	Reactome	R-HSA-388396	6	6/18	680/18873	8.45	0.002	0.009
Gs activates adenylyl cyclase	Reactome	R-HSA-163617	4	4/18	49/18873	22.51	0.002	0.012
Activated adenylyl cyclase catalyses cAMP synthesis	Reactome	R-HSA-164377	3	3/18	21/18873	19.74	0.004	0.016
PI3K–Akt signaling pathway	KEGG	hsa04151	4	4/18	354/18873	5.91	0.005	0.019
GLP-1 regulates insulin secretion	Reactome	R-HSA-381676	3	3/18	35/18873	14.04	0.006	0.021
Insulin signaling pathway	KEGG	hsa04910	3	3/18	133/18873	6.78	0.008	0.028
PKA activation	Reactome	R-HSA-163615	2	2/18	46/18873	12.19	0.013	0.033
PKA-mediated phosphorylation of CREB	Reactome	R-HSA-111931	2	2/18	14/18873	21.36	0.015	0.037
mTOR signaling pathway	KEGG	hsa04150	3	3/18	147/18873	5.98	0.017	0.041
FoxO signaling pathway	KEGG	hsa04068	3	3/18	128/18873	6.23	0.019	0.047

Note: The background for the hypergeometric test was the STRING human gene set. Query refers to GLP-1 module genes (n = 18) that were successfully mapped within the STRING (combined score ≥ 0.7) background (universe) and included in the enrichment analysis; the original definition of the GLP-1 module was 25 genes,and unmapped genes were automatically excluded during enrichment.

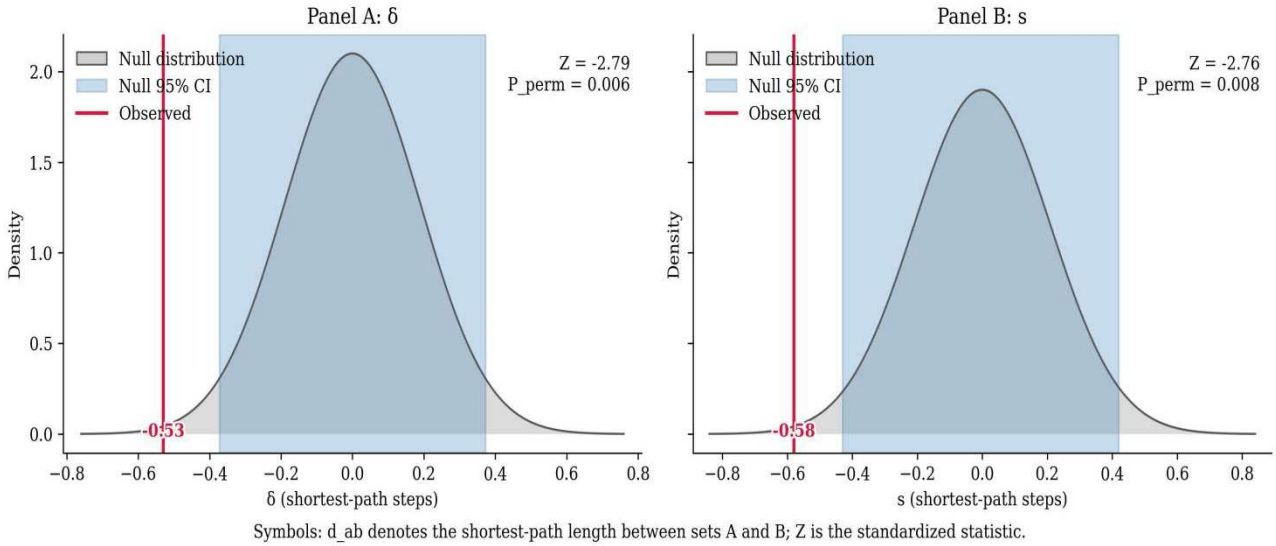

Fig. 6: Zero distributions and observed locations for δ and s

Table 4: List of key nodes ranked by shortest-path contribution

Node	Annotation	SPC (%)	Z score	P_perm
GNAS	Heterotrimeric G-protein Gs alpha subunit	38.26	4.21	0.001
PRKACA	Protein kinase A catalytic subunit alpha	33.41	3.78	0.002
CREB1	cAMP response element-binding transcription factor	31.07	3.45	0.004
ADCY5	Adenylate cyclase 5	27.92	3.09	0.007
ADCY3	Adenylate cyclase 3	24.68	2.86	0.011
PDE3B	Phosphodiesterase 3B (cAMP)	21.34	2.54	0.015
PRKAR2B	PKA regulatory subunit type II beta	19.87	2.31	0.019
GLP1R	Glucagon-like peptide-1 receptor	17.53	2.18	0.024
AKT1	Serine/threonine kinase AKT1 (PKBα)	15.66	2.04	0.037
PPARGC1A	PPAR gamma coactivator 1-alpha	14.22	1.98	0.044

Note: shortest-path contribution (SPC)

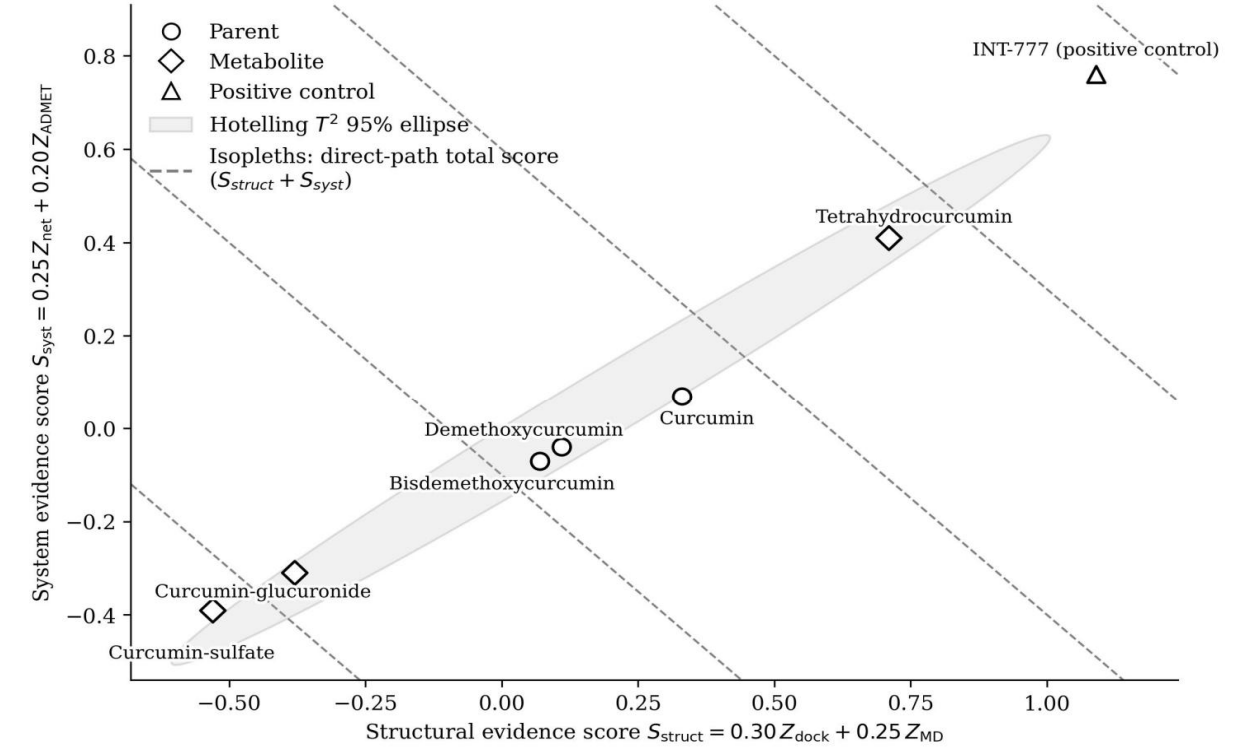

Symbols: $Z_{dock}, Z_{MD}, Z_{net}, Z_{ADMET}$ denote standardized scores for docking, MD, network, and ADMET, respectively.

Fig. 7: Structural vs. system evidence with Hotelling T² 95% ellipse

Publicly available TGR5 complex structures generally rely on hydrophobic clamping and limited polar anchor points to bind bile acid-like scaffolds; strong agonists exhibit higher hydrophobic occupancy and directional hydrogen bonds and the rule that natural small molecules have weak affinity and are sensitive to the membrane environment has also been widely substantiated (Chen G *et al*., 2020); the residue interaction pattern in this study is consistent with the above features and the directions of interaction of key sites such as W237, F96 and Y240 are also consistent with structural and mutagenesis evidence, providing concordant support at structural, dynamic and energetic levels for tetrahydrocurcumin as a direct ligand of TGR5 and clarifying specific targets and evaluation bases for subsequent validation under physiological membrane conditions and conformational ensembles. An integrated network presented a cascade centered on GNAS, with PRKACA and CREB1 as secondary hubs; TGR5 was directly connected to GNAS and GLP1R, together with GNAS and the adenylyl cyclase family, constituted the signaling backbone; functional enrichment highlighted cAMP signaling, Gαs-related events and GPCR downstream signaling, with shortest-path contributions concentrated on GNAS, ADCY isoforms, PRKACA and CREB1 and network proximity and separation both significantly below zero.

Table 5: ADMET prediction summary and composite receptor reachability score

Compound	Caco-2 logPapp (cm/s)	HIA probability (%)	P-gp substrate	CYP3A4 liability (prob.)	UGT liability (prob.)	LogS (mol/L)	LogP	PPB (%)	Metabolic stability	hERG risk (prob.)	Hepatotoxicity risk (prob.)	R_direct (0–1)	Interpretation
INT-777 (positive control)	-5.02	84.67	No	0.44	0.29	-5.78	3.18	91.22	High	0.07	0.12	0.78	Favorable
Tetrahydrocurcumin	-5.28	78.39	No	0.39	0.63	-5.12	2.81	89.47	Medium	0.06	0.08	0.64	Favorable
Curcumin	-5.71	42.18	Yes	0.62	0.87	-7.89	3.31	97.31	Low	0.11	0.09	0.47	Unfavorable
Demethoxycurcumin	-5.84	39.74	Yes	0.58	0.82	-7.42	3.78	96.12	Low	0.12	0.11	0.42	Unfavorable
Bisdemethoxycurcumin	-5.93	36.55	Yes	0.55	0.79	-8.21	4.02	98.06	Low	0.13	0.10	0.39	Unfavorable
Curcumin-glucuronide	-6.24	18.27	Yes	0.21	0.12	-3.24	1.58	78.35	Low	0.05	0.13	0.27	Unfavorable
Curcumin-sulfate	-6.31	16.88	Yes	0.18	0.09	-3.51	1.47	74.92	Low	0.06	0.14	0.23	Unfavorable

This topological pattern suggests that curcumin-related targets are in functional proximity to the GLP-1 module and genes related to T2DM with obesity *(Gan X et al., 2023)* and that signals are more likely to propagate along activation of adenylyl cyclase by Gαs to produce cAMP, relayed via PKA and CREB to secretory and metabolic endpoints, with PDE3B and PDE4B providing downstream braking sites *(Zheng Z et al., 2024)*; this structure provides network conditions for amplification of slight perturbations arising from TGR5 or its upstream and provides system-level support for computational evidence of enhancing endogenous GLP-1 signaling and improving insulin secretion; meanwhile, enrichment of the PI3K and Akt pathways suggests an expected bypass coupling with nodes of insulin sensitivity and lipid metabolism, leaving reasonable explanatory space for associations with obesity-related phenotypes *(Wen X et al., 2022)*. Existing studies indicate that GLP-1 secretion depends on cAMP elevation and PKA- and CREB-mediated transcriptional programs, bile acid receptor-mediated Gαs activation is a key prerequisite and GNAS occupies a central position in enteroendocrine cells and pancreatic islet cells *(Müller TD et al., 2019)*; adenylyl cyclase and the PDE family jointly determine cAMP homeostasis and PI3K and Akt signaling participate in regulation of the insulin pathway and energy metabolism *(Tomek J and Zaccolo M, 2023)*; the network fingerprint in this study was consistent with the above biological consensus and, in the absence of wet experiments, provided independent and mutually corroborative system-level evidence for the mechanistic feasibility and prioritization of linking curcumin to the GLP-1 axis via TGR5.

The R_direct score classified INT-777 and tetrahydrocurcumin as favorable, with the other molecules unfavorable; the two-dimensional positioning of the structural evidence score and the system evidence score was consistent with this, with the positive control in the upper right, tetrahydrocurcumin next, parent curcumin in the middle and conjugated metabolites with weak binding energy and deteriorated ADMET falling into the negative quadrant. The direct path candidate prioritization list formed thereby pointed to tetrahydrocurcumin, mechanistically supported by better pocket matching and a more balanced profile of permeability, efflux and metabolic stability, predicting relative reachability in achieving effective exposure at the basolateral side of the receptor *(Lok KH et al., 2022).*; the parent and its conjugated metabolites were limited by P-gp substrate status, low intestinal absorption and rapid metabolism, making it difficult to maintain effective occupancy *(Urošević M et al., 2022)*. The system network showed that the Gs–cAMP–PKA–CREB chain occupied an information amplification position, suggesting that even with moderate affinity, functional cascades may arise along this axis *(Yadav R and Zaccolo M, 2025)*. therefore tetrahydrocurcumin and its derivatives based on the hydrophobic triad and Y240 anchoring have greater

translational value, with priority consideration to achieving exposure enhancement through delivery system optimization, fine-tuning of the lipophilicity–polarity balance and efflux-avoidance strategies *(Moon DO, 2025)* Existing pharmacokinetic data on the low oral exposure of natural curcumin and the differential performance of metabolites are consistent with the above ranking direction and also support, under limited direct action evidence, parallel evaluation of bile acid–related indirect modulation pathways to construct testable translational hypotheses.

This study was computational and evidence integration and the conclusions point only to mechanistic feasibility and prioritization; they cannot be extrapolated to *in-vivo* efficacy and safety. Potential sources of bias involved PDB conformations and protonation choices, the force field and water model, docking and MM-PBSA approximations, the MD time scale, STRING edge confidence and GLP-1 module curation and ADMET model extrapolation; among these, R_direct is a heuristic composite indicator constructed based on *in-silico* ADMET predictors, used only for relative prioritization and not a substitute for measured data on (basolateral exposure) in intestinal L cells. Subsequent recommendations follow a minimal verification path: taking tetrahydrocurcumin as the primary object, set protein-binding-corrected concentrations in human L cells or GLP-1 reporter systems, with selective TGR5 antagonist or knockdown controls and FXR regulation controls and quantify cAMP and GLP-1 release; perform bidirectional permeability and efflux ratio assays in Caco-2 to evaluate basolateral reachability and conduct dissolution and stability testing under simulated physiological fluid conditions, combined with lipid delivery or solid dispersions to optimize exposure; repeat long-timescale molecular dynamics and perform free-energy sampling on membrane models containing cholesterol and different lipid components to verify the robustness of pocket occupancy and key interactions; measure bile acid profile changes in *in-vitro* microecology or metabolic systems to estimate the weight of indirect pathways and thereby refine the order of validation and preregistered endpoints.

CONCLUSION

Multi-layer computation and evidence integration indicated that curcumin modulating the GLP-1 pathway via TGR5 is mechanistically feasible and that a clear candidate prioritization can be formed. Structural, dynamic and energetic signals consistently supported direct binding with weak-to-moderate affinity, with tetrahydrocurcumin prioritized, parent curcumin in the middle and conjugated metabolites having a lower likelihood as direct ligands. The network system presented functional proximity of the Gs–cAMP–PKA–CREB backbone, suggesting that the endogenous GLP-1 axis is reachable via upregulatable pathways. ADMET and receptor reachability pointed to exposure and efflux as key constraints and the direct path was more likely to be realized by tetrahydrocurcumin. This chain of evidence supports the curcumin–TGR5–GLP-1 axis as a testable hypothesis and translational screening framework and does not point to conclusions on *in-vivo* efficacy.

Acknowledgement
We thank the Capital Health Development Research Special Project (Grant No. 2024-2-2236) for funding support.

Authors' contributions
Chengyi Zhao: Conception and design of study, acquisition of clinical data, data analysis, drafting of manuscript and critical revision of the manuscript; Juju Shang: Data analysis, critical revision of the manuscript and approval of the final version of the manuscript. All authors contributed to the revision and approval of the final submitted manuscript.

Funding
The Capital Health Development Research Special Project (Grant No. 2024-2-2236).

Data availability statement
All data generated or analysed during this study are included in this published article; and its supplementary information files.

Ethical approval
Not applicable.

Conflict of interest
The authors declare no competing interests.

Supplementary data
https://www.pjps.pk/uploads/2026/06/SUP1781005579.pdf

REFERENCES

American Diabetes Association Professional Practice Committee (2025). 8. Obesity and weight management for the prevention and treatment of type 2 diabetes: Standards of Care in Diabetes—2025. *Diabetes Care*, **48**(Suppl 1): S167-S180.

Bertoncini-Silva C, Vlad A, Ricciarelli R, Giacomo Fassini P, Suen VMM and Zingg JM (2024). Enhancing the bioavailability and bioactivity of curcumin for disease prevention and treatment. *Antioxidants (Basel)*, **13**(3): 331.

Brighton CA, Rievaj J, Kuhre RE, Glass LL, Schoonjans K, Holst JJ, Gribble FM and Reimann F (2015). Bile acids trigger GLP-1 release predominantly by accessing basolaterally located GPBAR1 (TGR5) on L-cells. *Endocrinology*, **156**(11): 3961-3970.

Chen G, Wang X, Ge Y, Ma L, Chen Q, Liu H, Du Y, Ye RD, Hu H and Ren R (2020). Cryo-EM structure of activated bile acids receptor TGR5 in complex with stimulatory G protein. *Signal Transduct Target Ther.*, **5**(1): 142.

Davies MJ, Aroda VR, Collins BS, Gabbay RA, Green J, Maruthur NM, Rosas SE, Del Prato S, Mathieu C, Mingrone G and Rossing P (2022). Management of hyperglycemia in type 2 diabetes, 2022: A consensus report by the American Diabetes Association (ADA) and the European Association for the Study of Diabetes (EASD). *Diabetes Care*, **45**(11): 2753-2786.

Eberhardt J, Santos-Martins D, Tillack AF and Forli S (2021). AutoDock Vina 1.2.0: New docking methods, expanded force field and Python bindings. *J Chem Inf Model*., **61**(8): 3891-3898.

Fleishman JS and Kumar S (2024). Bile acid metabolism and signaling in health and disease: Molecular mechanisms and therapeutic targets. *Signal Transduct Target Ther*., **9**: 97.

Gan X, Shu Z, Wang X, Yan D, Li J, Ofaim S, Albert R, Li X, Liu B, Zhou X and Barabasi AL (2023). Network medicine framework reveals generic herb-symptom effectiveness of traditional Chinese medicine. *Sci Adv*., **9**(43): eadh0215.

Gonzalez Y, Mojica-Flores R, Moreno-Labrador D, Pecchio M, Rao KJ, Ahumedo-Monterrosa M, Fernandez PL, Larionov OV and Lakey-Beitia J (2023). Tetrahydrocurcumin derivatives enhanced the anti-inflammatory activity of curcumin: Synthesis, biological evaluation and structure–activity relationship analysis. *Molecules*, **28**(23): 7787.

He Y, Chen X, Li Y, Liang Y, Hong T, Yang J, Cao Z, Mai H, Yao J, Zhang T and Wu K (2024). Curcumin supplementation alleviates hepatic fat content associated with modulation of gut microbiota–dependent bile acid metabolism in patients with nonalcoholic simple fatty liver disease: A randomized controlled trial. *Am J Clin Nutr*., **120**(1): 66-79.

Jin W, Zheng M, Chen Y and Xiong H (2024). Update on the development of TGR5 agonists for human diseases. *Eur J Med Chem*., **271**: 116462.

Leidner F, Kurt Yilmaz N and Schiffer CA (2019). Target-specific prediction of ligand affinity with structure-based interaction fingerprints. *J Chem Inf Model*., **59**(9): 3679-3691.

Lok KH, Wareham NJ, Nair RS, How CW and Chuah L-H (2022). Revisiting the concept of incretin and enteroendocrine L-cells as type 2 diabetes mellitus treatment. *Pharmacol Res*., **180**: 106237.

Ma L, Yang F, Wu X, Mao C, Guo L, Miao T, Zang SK, Jiang X, Shen DD, Wei T and Zhou H (2022). Structural basis and molecular mechanism of biased GPBAR signaling in regulating NSCLC cell growth via YAP activity. *Proc Natl Acad Sci USA*, **119**(29): e2117054119.

Moon DO (2025). Structure-Based Insights into TGR5 Activation by natural compounds: Therapeutic implications and emerging strategies for obesity management. *Biomedicines*, **13**(10): 2405.

Muller TD, Finan B, Bloom SR, D'Alessio D, Drucker DJ, Flatt PR, Fritsche A, Gribble F, Grill HJ, Habener JF and Holst JJ (2019). Glucagon-like peptide 1 (GLP-1). *Mol Metab*., **30**: 72-130.

Panossian A (2025). Trends and pitfalls in the progress of network pharmacology research on natural products. *Pharmaceuticals (Basel)*, **18**(4): 538.

Pinero J, Ramirez-Anguita JM, Sauch-Pitarch J, Ronzano F, Centeno E, Sanz F and Furlong LI (2020). The DisGeNET knowledge platform for disease genomics: 2019 update. *Nucleic Acids Res*., **48**(D1): D845-D855.

Rodriguez PJ, Zhang V, Gratzl S, Do D, Goodwin Cartwright B, Baker C, Gluckman TJ, Stucky N and Emanuel EJ (2025). Discontinuation and reinitiation of dual-labeled GLP-1 receptor agonists among US adults with overweight or obesity. *JAMA Netw Open*, **8**(1): e2457349.

Tian F, Chen T, Xu W, Fan Y, Feng X, Huang Q and Chen J (2023). Curcumin compensates GLP-1 deficiency via the microbiota-bile acids axis and modulation in functional crosstalk between TGR5 and FXR in ob/ob mice. *Mol Nutr Food Res*., **67**(22): e2300195.

Torrens-Fontanals M, Stepniewski TM, Aranda-Garcia D, Morales-Pastor A, Medel-Lacruz B and Selent J (2020). How do molecular dynamics data complement static structural data of GPCRs. *Int J Mol Sci*., **21**(16): 5933.

Tomek J and Zaccolo M (2023). Compartmentalized cAMP signalling and control of cardiac rhythm. *Philos Trans R Soc Lond B Biol Sci*., **378**(1879): 20220172.

Urosevic M, Nikolic L, Gajic I, Nikolic V, Dinic A and Miljkovic V (2022). Curcumin: Biological activities and modern pharmaceutical forms. *Antibiotics (Basel)*, **11**(2): 135.

Wen X, Zhang B, Wu B, Xiao H, Li Z, Li R, Xu X and Li T (2022). Signaling pathways in obesity: Mechanisms and therapeutic interventions. *Signal Transduct Target Ther*., **7**(1): 298.

Yang F, Mao C, Guo L, Lin J, Ming Q, Xiao P, Wu X, Shen Q, Guo S, Shen DD and Lu R (2020). Structural basis of GPBAR activation and bile acid recognition. *Nature*, **587**(7834): 499-504.

Yadav R and Zaccolo M (2025). GPCR signaling via cAMP nanodomains. *Biochem J*., **482**(10): 519-533.

Zheng L, Meng J, Jiang K, Lan H, Wang Z, Lin M, Li W, Guo H, Wei Y and Mu Y (2022). Improving protein–ligand docking and screening accuracies by incorporating a scoring function correction term. *Brief Bioinform*., **23**(3): bbac051.

Zheng Z, Zong Y, Ma Y, Tian Y, Pang Y, Zhang C and Gao J (2024). Glucagon-like peptide-1 receptor: Mechanisms and advances in therapy. *Signal Transduct Target Ther*., **9**(1): 234.